Cell Reports
Methods

Article

Continuous monitoring of multiple biomarkers with an ultrasensitive 3D-structured wearable biosensor

Graphical abstract

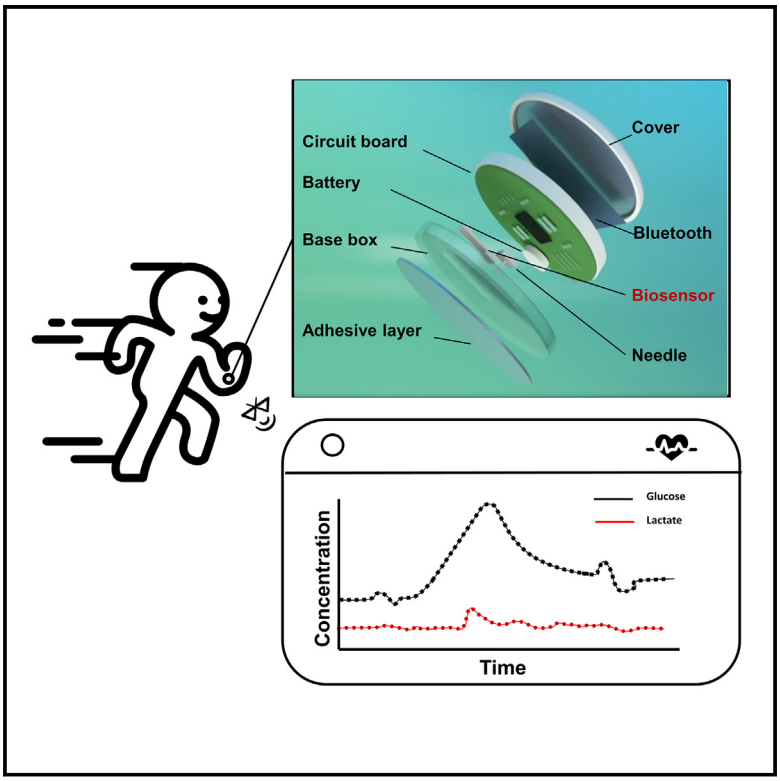

Authors

Muqun Yang, Han Wang, Jing Cheng

Correspondence

hanwang@tsinghua.edu.cn (H.W.),
jcheng@tsinghua.edu.cn (J.C.)

In brief

Yang et al. present a fully integrated wearable system with an ultrasensitive 3D-structured biosensor for real-time monitoring of multiple metabolites for disease management. The proposed system demonstrates superior sensitivity and selectivity in glucose and lactate sensing. Furthermore, *in vivo* animal experiments have been conducted to validate its potential for clinical applications.

Highlights

- The fully integrated wearable device monitors multiple metabolites dynamically
- The device features an ultrasensitive dual-channel 3D-structured biosensor
- The proposed biosensor possesses superior sensitivity and selectivity
- The device provides dynamic trends of metabolites in ISF for disease management

Yang et al., 2023, Cell Reports Methods *3*, 100579
September 25, 2023
https://doi.org/10.1016/j.crmeth.2023.100579

CellPress

Cell Reports Methods

CellPress
OPEN ACCESS

Article

Continuous monitoring of multiple biomarkers with an ultrasensitive 3D-structured wearable biosensor

Muqun Yang,[1,2] Han Wang,[2,4,*] and Jing Cheng[2,3,*]

[1]Precision Medicine and Healthcare Research Center, Tsinghua-Berkeley Shenzhen Institute (TBSI), Tsinghua University, Shenzhen 518055, China

[2]Department of Biomedical Engineering, School of Medicine, Tsinghua University, Beijing 100084, China

[3]National Engineering Research Center for Beijing Biochip Technology, Beijing 102206, China

[4]Lead contact

*Correspondence: hanwang@tsinghua.edu.cn (H.W.), jcheng@tsinghua.edu.cn (J.C.)

https://doi.org/10.1016/j.crmeth.2023.100579

MOTIVATION The management of chronic diseases requires routine monitoring of specific biomarkers. However, traditional *in vitro* diagnostic technologies suffer from complex sampling processes and long detection intervals and only allow for single-analyte detection, which is not practical in home-based health management. Wearable devices taking advantage of compact size, rapid detection process, easy integration, and small sample consumption are promising to take the place of endpoint detection, providing more comprehensive information about human health. Thus, a wearable device based on a dual-channel biosensor for continuous, real-time monitoring of multiple metabolites was developed in this work to address the existing limitations.

SUMMARY

Chronic diseases call for routine management of frequent monitoring of specific biomarkers. Traditional *in vitro* diagnostics technologies suffer from complex sampling processes and long detection intervals, which cannot meet the need of continuous monitoring. Wearable devices taking advantage of compact size, rapid detection process, and small sample consumption are promising to take the place of endpoint detection, providing more comprehensive information about human health. Here, we proposed a fully integrated wearable system with an ultrasensitive 3D-structured biosensor for real-time monitoring of multiple metabolites. The 3D-structured biosensor shows wide linear ranges of 400–1,400 μM and 0.1–8 mM and high sensitivities of 460.5 and 283.09 $\mu A/(mM \cdot cm^2)$ for lactate and glucose detection, respectively. We have conducted *in vivo* animal experiments, and the proposed wearable biosensor demonstrated high consistency with established methods. We envision that this system could provide a real-time wearable detection platform for multiple biomarker detection.

INTRODUCTION

Diabetes mellitus, as one of the most prevalent and serious chronic diseases, was responsible for 6.7 million deaths in 2021 all over the world.[1] Patients with diabetes mellitus suffer from insulin deficiency or insulin resistance, which both lead to abnormal levels of blood glucose. Lasting high blood glucose levels in the human body may cause irreversible damage to nerves and blood vessels, giving rise to more than 100 kinds of diabetic complications and endangering the heart, brain, kidney, eyes, feet, and so on.[2] Thus, maintaining glucose levels within an appropriate range is vital for diabetes control and health management, which calls for routine blood glucose monitoring and antidiabetic agent administration. However, commonly used antidiabetic agents usually enhance anaerobic glycolysis or cast down gluconeogenesis, which may lead to increased blood lactate levels. Together with naturally accumulated glycated hemoglobin, which will significantly aggravate and accelerate the lactate production by intensifying anaerobic glycolysis, the blood lactate level is frequently elevated in patients with diabetes, causing hyperlactatemia and lactic acidosis without noticeable symptoms.[3] Thus, dynamic monitoring and regulating blood lactate levels in real time is also indispensable for managing diabetic complications. Therefore, simultaneous monitoring of blood glucose and lactate levels are of great importance in evaluating the health status and managing diabetes progression.

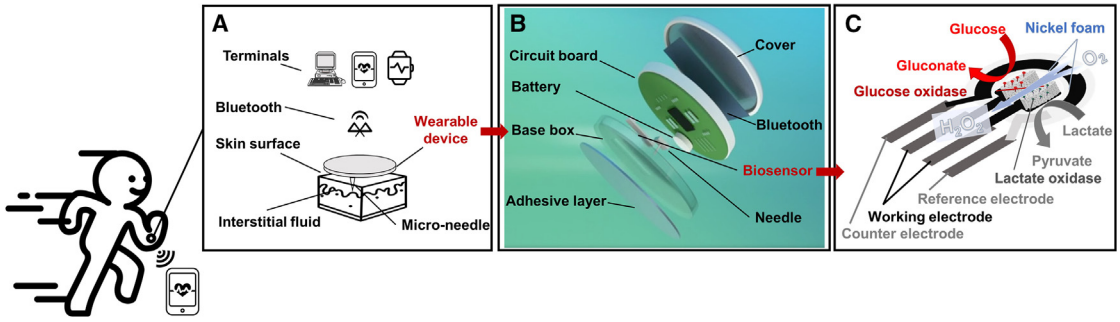

Figure 1. Schematic illustration of the wearable system for multiple-metabolite monitoring

(A) Diagram of the wearable system for multiple-metabolites monitoring. A microneedle is applied to obtain interstitial fluid, and the analyte was tested by the biosensor. Later, the data were sent to the terminals via Bluetooth.

(B) Diagram of the wearable system for multiple-metabolite monitoring. It consists of five parts: an MCU module, a potentiostat module, a data transmission module, a data processing module, and an electrochemical biosensor module.

(C) Construction of the dual-channel 3D-structured nickel foam biosensor. The biosensor contains two working electrodes, one reference electrode and one counter electrode. The nickel foam working electrodes were modified with glucose oxidase and lactate oxidase, respectively.

Over the past decades, various methods have emerged to detect biochemical markers such as glucose and lactate, including colorimetry,[4] chemiluminescence,[5] high-performance liquid chromatography,[6] and enzymatic fluorescence.[7] Although these methods are sensitive and reliable, they suffer from complex sampling pre-treatment, long detection times and the requirement of cumbersome instruments, which cannot meet the demand for real-time tracking of the dynamic change of glucose and lactate levels and may miss plenty of critical information such as transient fluctuation of metabolite levels out of normal ranges.[8] Electrochemical detection methods with high sensitivity, rapid response, and flexibility of integration have emerged and have become mainstream techniques for biochemical molecule detection.[9] Therefore, conceiving novel devices based on electrochemical technology for real-time monitoring of glucose and lactate levels is feasible and vital.

Wearable devices, taking advantage of their compact size, comfortable attachment, long working life, and small sample consumption, show promising applications in routine monitoring of metabolite levels without causing discomfort or interruptions to daily activity.[10,11] So far, a handful of miniaturized wearable devices have been developed, such as the epidermal patch for multiple metabolite detection,[12] the tattoo-based biosensor for sweat testing,[13] and skin-like sensors (SLSs) for multimodal signal monitoring including bioelectric and biomechanical signals.[14] However, these wearable biosensors applied only to the body fluid detection on the surface of epidermis, suffering from low sensitivity and poor accuracy caused by individual

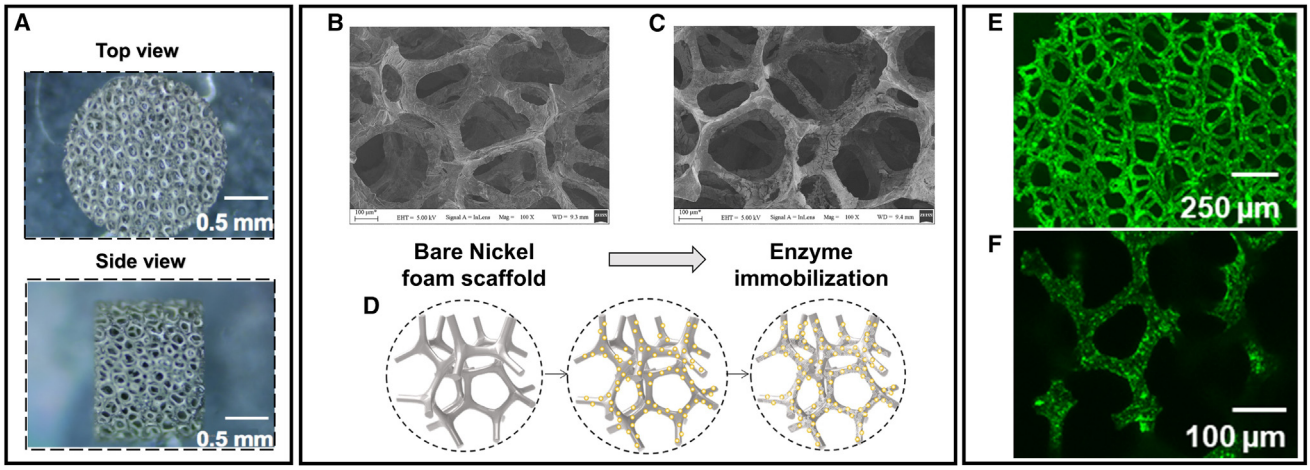

Figure 2. Property characterization of nickel foam electrode

(A) Top view and side view of modified nickel foam. Scale bar: 0.5 mm.

(B) SEM imagine of bare nickel foam electrode. Scale bar: 100 μm.

(C) SEM imagine of enzyme-modified nickel foam electrode. Scale bar: 100 μm.

(D) Schematic diagram of the fabrication and application of the enzyme-modified nickel foam electrode.

(E) Confocal microscopy image of enzyme-modified dual-channel nickel foam electrode. Scale bar: 250 μm.

(F) Confocal microscopy image of enzyme-modified dual-channel nickel foam electrode. Scale bar: 100 μm.

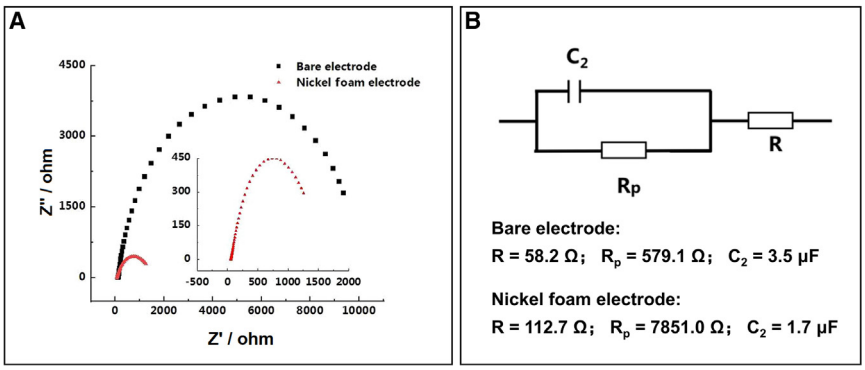

Figure 3. Interface impedance characterization of nickel foam electrode

(A) Nyquist plots of EIS results of the bare electrode and the nickel foam modified electrode. The insert shows the enlarged view of the EIS results of the nickel foam-modified electrode.

(B) Calculated parameters of the equivalent circuit fitting with the measured data from the Chenhua electrochemical workstation.

variance and environmental changes. Besides, limited by the intermittent secretion of body fluids, wearable biosensor patches have difficulty to collecting continuous metabolite information, leading to the omission of key points or the absence of transient outrange values. Therefore, developing minimally invasive devices to collect high-quality dynamic changes of metabolite levels is of great importance.

Recently, minimally invasive continuous glucose monitoring (CGM) systems that can achieve metabolite analysis with interstitial fluid (ISF) and provide accurate and dynamic metabolite information, have been put forward and have attracted widespread attention. However, these CGM systems still suffer from high cost and low sensitivity and can only realize the detection of a single metabolite. Recently, Tehrani et al.[15] reported a fully integrated, wireless continuous monitoring system for ISF biomarkers, that can realize real-time sensing of two metabolites through the wearable microneedle array. However, this system has disadvantages of limited stability for only a few hours and a complicated fabrication process, making the system unsuitable for daily use and long-term monitoring. Therefore, developing a wearable CGM device with high sensitivity, good stability, low cost, simple processing steps, and negligible crosstalk for simultaneous monitoring of multiple metabolites is of great importance.

Here, we propose a fully integrated wearable biosensing device with an ultrasensitive 3D-structured biosensor for continuous real-time monitoring of multiple metabolites in ISF. The device consists of a sample collection module, a biosensing module, a signal processing module, and so on. The biosensing module is fabricated with a cost-effective movable-type bioelectronics printing method[16] and finally integrated with enzyme-modified 3D-structured nickel foams on the working electrodes. All the modules, including sensors, micro control unit (MCU), data processing modules, wireless communication modules, power management modules, etc., are compatibly integrated as a wearable device. This wearable biosensing device benefits from the following aspects. Firstly, the biosensors with 3D-structured electrodes could provide high specific surface area, high electro-catalytic activity and large contact area with samples, which could significantly improve the sensitivity of these biosensors.[17,18] Secondly, the developed biosensor on our platform for monitoring of multiple metabolites uses a shared counter electrode and reference electrode, greatly simplifying the peripheral circuit and reducing its footprint in integration and fabrication. Besides, the developed biosensor could be easily replaced or expanded to realize simultaneous monitoring of a variety of metabolites, such as glucose, lactate, uric acid, cortisol, and other biomolecules, providing a general method for accurate metabolite detection. Thirdly, this monitoring system working with a portable and minimized potentiostat can provide actionable information on the dynamic trend of metabolites in a wearable fashion for improved disease management. In summary, we developed a wearable device for accurate and real-time monitoring of multiple metabolites. To assess the performance of this wearable device, we have conducted *in vivo* animal experiments and compared the results with gold-standard measurements in blood for simultaneous monitoring of glucose and lactate. We envision that this system could provide a wearable real-time monitoring platform for electrochemical detection of multiple biomolecules.

RESULTS

System design and construction of the biosensor

The developed ultrasensitive dual-channel biosensor is based on the enzyme-modified 3D-structured nickel foam electrode interface. On the one hand, 3D-structured nickel foam provides high specific surface area, high electro-catalytic activity, and large contact area with samples, endowing the biosensor with excellent electron conductivity and superior sensitivity. On the other hand, specific enzymes attached to the surface of the 3D-structured nickel foam can specifically catalyze redox reactions of the target metabolites, greatly improving the selectivity and accuracy of the dual-channel biosensor in complex biological fluids. Finally, the developed ultrasensitive dual-channel biosensor is integrated in a single three-electrode electrochemical system. The two separate sensing interfaces share the counter electrode and reference electrode during detection, notably simplifying the peripheral circuit and facilitating the miniaturization of the wearable system.

Figures 1A and 1B show the schematics of the fully integrated wearable device. The device consists of six modules including the adhesive layer, a base box, a dual-channel biosensor, a microneedle, a circuit board, and a cover, which can detect and transmit real-time data to electronic terminals such as cell phones, watches, personal computers, and so on. Figure 1C shows the configuration of the developed enzyme-modified dual-channel 3D-structured nickel foam biosensor based on

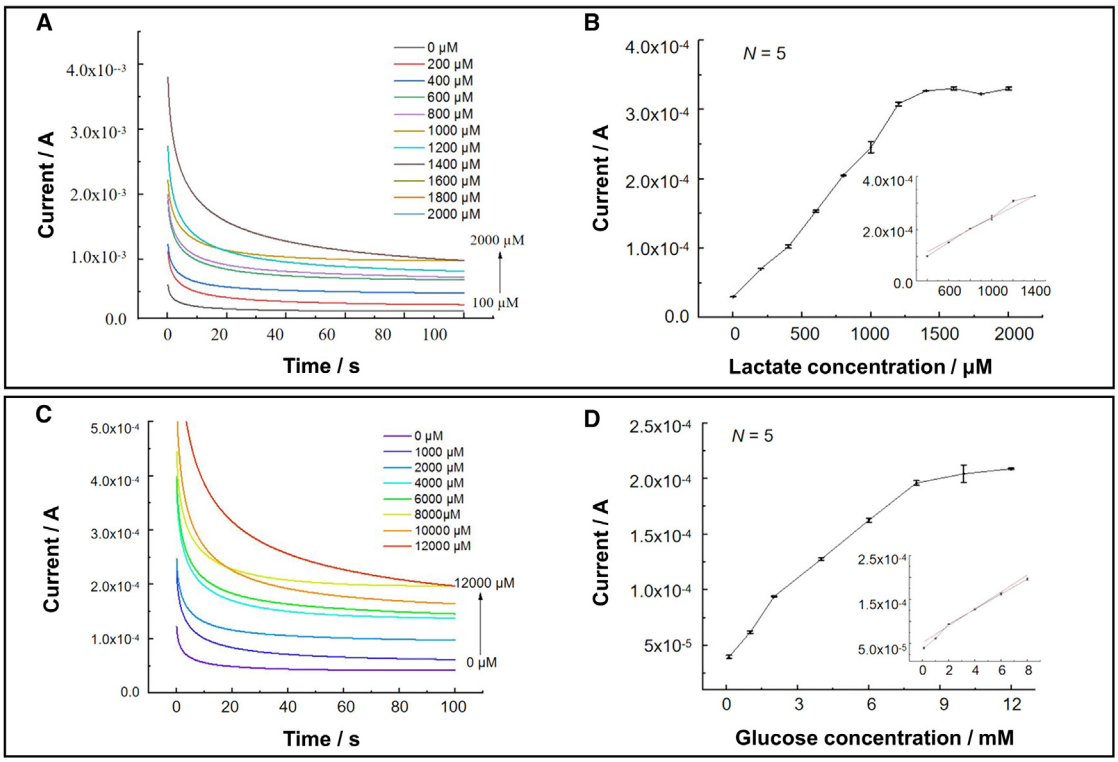

Figure 4. Sensitivity characterization of dual-channel nickel foam biosensor for lactate and glucose detection

(A) The i-t curves of lactate at different concentrations.

(B) Stable i-t values plotted as functions of lactate concentrations (n = 5). Inset is the linear curve fitting between currents and lactate concentrations, coefficient of association R^2 = 0.9905. The linear range was 400–1,400 μM, and the sensitivity was 460.5 μA/(mM×cm^2) (the area of the working electrode was 0.05 cm^2).

(C) The i-t curves of glucose at different concentrations.

(D) Stable i-t values plotted as functions of glucose concentrations (n = 5). Inset is linear curve fitting between currents and glucose concentration, coefficient of association R^2 = 0.9886 (n = 5). The linear range was 0.1–8 mM and the sensitivity was 378.3 μA/(mM×cm^2) (The area of the working electrode was 0.05 cm^2).

the three-electrode scheme. The biosensor possesses two working electrodes in a shared three-electrode system, which can detect glucose and lactate, respectively.

As seen from Figure 2A, the surface of the working electrode was covered by 3D-structured porous, sponge-like nickel foam. The average size of the pores in the nickel foam scaffold was calculated to be 96 μm, and the porosity was determined to be 77.8%. Additionally, the pores per line inch (PPI) of the nickel foam scaffold was up to 100, providing sufficient specific surface area to immobilize enzymes and increase the contact area between the electrode and the analyte solution. Figures 2B and 2C) show the scanning electron microscopy (SEM) images of the developed 3D-structured nickel foam electrode before and after enzyme immobilization. The enzyme immobilization process mainly includes enzyme adsorption and crosslinking (Figure 2D; STAR Methods). After the immobilization of glucose oxidase and lactate oxidase, the inside and the surface of the nickel foam were evenly covered by clusters of ellipsoidal particles, as can be seen from confocal images (Figures 2E and 2F), suggesting stable immobilization and effective dispersion of the enzymes with negligible influence to the structure of nickel foam scaffold.

Electrochemical characterization of the dual-channel 3D-structured nickel foam biosensor

The electrochemical performance of the bare dual-channel electrode and the developed dual-channel 3D-structured nickel foam electrode was first evaluated by electrochemical impedance spectroscopy (EIS) testing. EIS results of the bare electrode and the nickel foam-modified electrode were plotted, and the equivalent circuit parameters were calculated. As shown in Figure 3, the polarization resistances (Rps) were determined to be 579.1 Ω in the 3D-structured nickel foam electrode and 7,851.0 Ω in the bare electrode, demonstrating outstanding electroconductibility of the developed dual-channel 3D-structured nickel foam electrode. The standard errors of equivalent circuit fitting of the bare electrode and the 3D-structured nickel foam electrode were 8.3×10^{-9} and 2.6×10^{-6}, respectively, which suggested that the equivalent circuits well fit the Nyquist plot.

Performance of the dual-channel 3D-structured nickel foam biosensor

The amperometric (i-t) curves and the corresponding linear fitting curves for detection of glucose and lactate solutions at various concentrations are presented in Figure 4, respectively. The

Table 1. Comparison of the analytical performance of the 3D-structured nickel foam biosensor in this work with other electrochemical sensors

Electrode	Linear range	Sensitivity/$\mu A/(mM \cdot cm^2)$	LOD/μM	Ref.
Glucose				
GOx/gold/MoS_2	10–500 nM	–	0.01	Majumdar and Mahanta[19]
GOx/TiO_2/PAni	20–140 μA	163.14	0.533	Puttananjegowda et al.[20]
GOx/ENFM/SiCNPs	0.5–20 mM	30.75	0.56	Cai et al.[21]
PB ink/PAni/GOx/PU	0-12 mM	16.66	–	Popov et al.[22]
GOx/PAni/rGO	0.5–50 mM	2.8	89	Liu et al.[23]
This work	0.1-8 mM	283.09	1.54	–
Lactate				
LOx/Pt-G/PEN	0.4–6 mM	6.68	–	Madden et al.[24]
LOx/Pt-chitosan/LIG	0.2–3 mM	35.8	110	Han et al.[25]
LOx/PdCu/LIG	0.1–30 mM	51.91	–	Tsou et al.[26]
LOx/NiOx-Nafion	0.5–4 mM	205.6	270	Neampet et al.[27]
LOx/Pt/PANI/MXene	0.005–5.0 mM	5.64	5	Heikenfeld et al.[28]
This work	0.4–1.4 mM	460.5	40	–

results indicated that the dual-channel 3D-structured nickel foam biosensor possessed a wide linear range and high sensitivity in glucose and lactate detection. As shown in Figures 4A and 4B, the response current increased gradually as the concentration of lactate increased from 400 to 1,400 μM. A similar phenomenon was observed for glucose detection in Figures 4C and 4D, with a linear range of 0.1–8 mM. According to the measured results, the sensitivity of lactate detection in PBS medium was 460.5 $\mu A/((mM \times cm^2))$, while for glucose detection the sensitivity was 378.3 $\mu A/(mM \times cm^2)$, which outperformed most of the previously reported electrochemical biosensors (Table 1), and satisfied the requirement of clinical lactate and glucose detection in ISF.

Design and characterization of a potentiostat integrated with the biosensor

According to the equivalent circuit of the dual-channel 3D-structured nickel foam biosensor, we designed and fabricated a potentiostat connected to the three-electrode biosensor. The simulation results of the potentiostat can be found in Figure S1, where the experimental values of the potentiostat (seen from Table S1) were approximately equal to the theoretical values, proving the feasibility of the designed potentiostat.

Additionally, to assess the accuracy of our designed potentiostat integrated with the dual-channel 3D-structured nickel foam biosensor, we applied both the developed potentiostat and a commercial electrochemical workstation to work with the three-electrode biosensor to compare their performances in cyclic voltammetry (CV) and i-t curve measurements. As shown in Figure 5A, CV curves from our developed potentiostat and commercial electrochemical workstation matched well. As calculated, the main parameters for CV testing including the peak potential and peak current corresponding to oxidation and reduction processes, measured by the developed signal processing system and by the Chenhua electrochemical workstation, were highly consistent (Figure 5B) with a deviation of less than 2% (Table S2). Additionally, as can be seen from Figures 5C and 5D, the i-t curves at different glucose concentrations match well between these two detection systems ($p = 0.727$, paired t-test). These results demonstrated that our detection system was capable of performing CV or i-t curve detection accurately with the electrochemical biosensor, holding great potential in the construction of a fully integrated wearable device for real-time metabolite monitoring.

Dynamic monitoring and in *vivo* detection of the fully integrated wearable device

The integrated wearable device works with a sample collection module, a biosensing module, and a signal processing module to realize dynamic metabolite monitoring (see Figure 6A). To be specific, the system applied a microneedle to obtain the ISF sample, and the analyte solution was tested by the dual-channel 3D-structured nickel foam biosensor. The electrochemical signal was rapidly processed and sent to electronic terminals like cell phones, smart watches, computers and so on via Bluetooth. Figure 6B shows the i-t curves of dynamic measurement of lactate and glucose solutions using the developed device with the dual-channel 3D-structured nickel foam biosensor. PBS solutions containing lactate at different concentrations ranging from 0 to 1,800 μM with an interval of 200 μM were tested continuously, simulating the dynamic secretion of lactate *in vivo*. Similar experiments were also conducted in those solutions containing glucose at different concentrations ranging from 0 to 12 mM with an interval of 2 mM. The amplitudes of response currents increased rapidly as the concentrations of lactate or glucose went up, demonstrating the sensing capability of the detection system with the dual-channel biosensor that can facilitate dynamic monitoring of both lactate and glucose.

To confirm the feasibility of the developed wearable device for dynamic *in vivo* measurement of lactate and glucose levels, animal experiments were conducted. Since the concentration of glucose and lactate proved to be closely correlated in ISF and blood,[29] we compared the glucose and lactate levels in

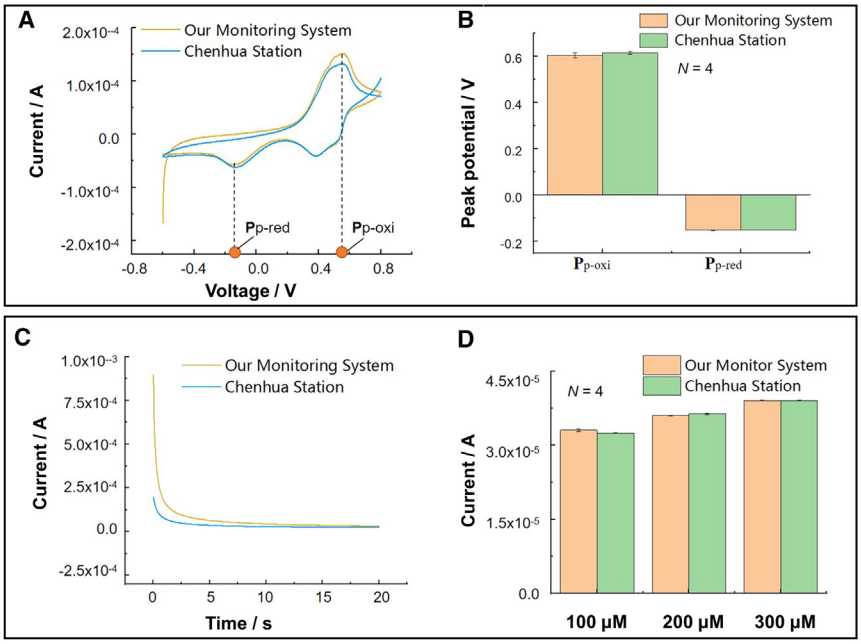

Figure 5. Performance characterization of our developed electrochemical station

(A) Two CV curves detected by our system and the commercial electrochemical station in $K_3[Fe(CN)_6]$ solution.

(B) Comparison of the peak potential of oxidation (Pp_oxi) and peak potential of reduction (Pp_red) measured by our system and the commercial electrochemical station. (n = 4, P(Pp_oxi) = 0.092, paired t-test; P(Pp_red) = 0.252, paired t-test).

(C) Two i-t curves detected by our system and the commercial electrochemical station.

(D) Comparison of the response current by our system and the commercial electrochemical station with different concentrations of $K_3[Fe(CN)_6]$ solution (100, 200, and 300 μM). (n = 4, p = 0.727, paired t-test).

ISF detected by the wearable system with the glucose and lactate levels in blood detected by commercial meters. Through these tests, the performance of our designed system in routine monitoring could be evaluated, and its potential in predicting blood glucose and lactate concentrations through ISF measurement was assessed. To be specific, the lactate and glucose levels in interstitial fluid of a healthy mouse were tested with our wearable device (seen from Figure 6C), and compared with those in tail blood measured by commercial electrochemical analyzers, ACCU-CHEK for glucose and Lactate Scout 4 for lactate. The trend of measured lactate and glucose concentrations matched well between ISF test by the wearable system and the tail blood test by commercial analyzers with correlations of 0.994 and 0.971 for lactate and glucose, respectively (Figure 6D), proving the feasibility of the wearable system in simultaneous monitoring of glucose and lactate levels *in vivo*, and the utility to evaluate the dynamic change of blood glucose and lactate levels through minimally invasive ISF monitoring.

DISCUSSION

In this work, we developed a fully integrated wearable system with enhanced accuracy and multimetabolite sensing capability. The dual-channel 3D-structured nickel foam biosensor exhibited outstanding performance with wide linear ranges of 400–1,400 μM and 0.1–8 mM and high sensitivities of 460.5 and 283.09 $\mu A/(mM \cdot cm^2)$ for lactate and glucose detection, respectively, which satisfies the need of glucose and lactate detection in real ISF. We have designed and simulated a potentiostat according to the equivalent circuit of the biosensor, which showed high consistency with the electrochemical workstation. Furthermore, a dual-channel biosensor for glucose and lactate detection was fabricated by bioelectronics printing technology and connected with our detection system. Finally, *in vivo* animal tests proved the functionality of the wearable device in simultaneous monitoring of glucose and lactate in ISF, which could reflect the dynamic change of glucose and lactate levels in blood.

In conclusion, we have successfully developed a fully integrated wearable device with an ultrasensitive 3D-structured biosensor for continuous monitoring of multiple biomarkers. The proposed wearable system possesses the following advantages. Firstly, the enzyme-modified 3D-structured nickel foam electrode exhibited outstanding electrocatalytic activity toward glucose and lactate detection through the unique hollow sphere surface morphology. The nickel foam electrode held the merits of highly exposed enzyme immobilization sites, high conductivity and large electrochemical active surface area, endowing the biosensor with superior sensitivity and selectivity. Secondly, the developed ultrasensitive dual-channel biosensor was integrated in a single three-electrode electrochemical system. The two separate sensing interfaces shared the counter electrode and reference electrode during detection, notably simplifying the peripheral circuit and facilitating miniaturization of the wearable system. Besides, the developed biosensor on our platform could be easily replaced or expanded to realize simultaneous monitoring of a variety of metabolites, such as glucose, lactate, uric acid, cortisol, and other biomolecules, providing a general approach for multimetabolite detection. Thirdly, this real-time monitoring system works with a portable and accurate potentiostat that can provide actionable information on the dynamic trend of metabolites in ISF in a minimally invasive fashion for improved disease management. In summary, we have developed a wearable device for accurate and real-time monitoring of multiple metabolites, which may expand the potential applications of wearable devices for digital healthcare.

All in all, the development of such a fully integrated, dual-channel ultrasensitive and dynamic monitoring system enriches the functionalities and potentials of wearable devices and opens the door to numerous wearable healthcare

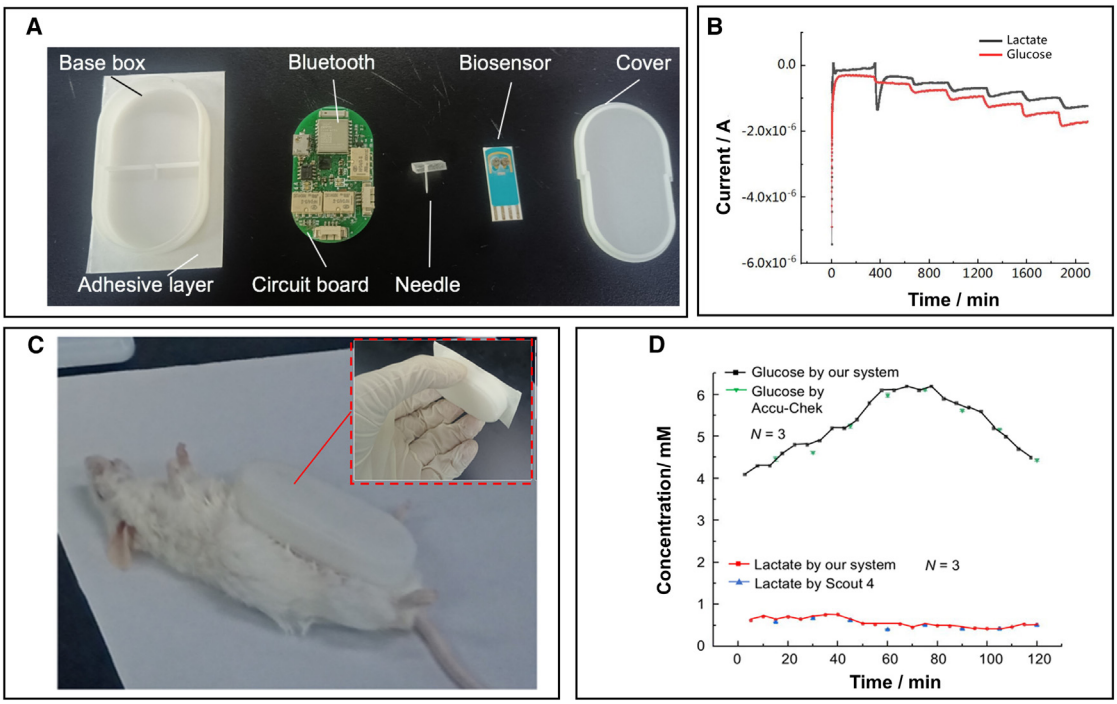

Figure 6. Dynamic detection capability verification of the wearable system by *in vivo* test

(A) Photograph of the main components of our monitoring system with a dual-channel biosensor. The size of the device was 3×5×0.5 (cm^3), and its total weight was 40 g. The working time of the device was 3 days with a button battery. Terminals such as cell phones, smart watches, computers, etc., could be utilized to acquire real-time monitoring data.

(B) I-t curve for dynamic measurement of lactate and glucose solution with the biosensor. The concentration gradients of lactate and glucose samples ranged from 0 to 300 μM with an interval of 50 μM.

(C) The photograph of the wearable device attached to a healthy mouse, while the inset shows the photograph of the integrated wearable devices.

(D) Comparison results between our system with two commercial devices. The black line and green dots represent the glucose levels measured by our system and the Accu-Chek, respectively (n = 3), and the red line and blue dots represent the lactate levels measured by our system and the Scout 4, respectively (n = 3). The statistical analysis showed no significant difference between interstitial fluid results by the wearable system and blood test results by commercial devices (paired t-test, $p > 0.05$).

possibilities, empowering future development of digital medicine. By moving the biological interface of wearable devices from the epidermis into subcutaneous tissue and expanding the sensing capability from single-analyte detection to multiple-target monitoring, we envision that the proposed wearable ultrasensitive metabolite monitoring system will accelerate the emergence of next-generation continuous monitoring wearable sensors and thereby offer a pathway to transform digital healthcare.

Limitations of the study

In this work, a fully integrated wearable system with enhanced accuracy and multimetabolite sensing capability was developed. However, there still exists several limitations that may hinder its practical application. For one thing, enzymatic electrochemical biosensors for metabolite sensing inevitably face the problems of enzyme loss or inactivation, leading to limited lifespan of the device and gradual degradation in the performance of metabolite detection over time. For another, the diffusion-based ISF detection approach makes the detection interval of the device greatly affected by the sampling efficiency, which leads to limited detection frequency and susceptibility to environmental disturbance. Thus, in the future, further research could be conducted to address these limitations, including exploring alternative sensing mechanisms, developing strategies to enhance enzyme stability, and optimizing the ISF sampling techniques to achieve long-term dynamic monitoring.

STAR★METHODS

Detailed methods are provided in the online version of this paper and include the following:

- KEY RESOURCES TABLE
- RESOURCE AVAILABILITY
  - Lead contact
  - Materials availability
  - Data and code availability
- EXPERIMENTAL MODEL AND STUDY PARTICIPANT DETAILS
- METHOD DETAILS
  - Electrochemical detection mechanism of the 3D-structured nickel foam electrode

- Fabrication of the dual-channel 3D-structured biosensors through a movable type bioelectronics printing technology
- Enzyme modification of dual-channel 3D-structured biosensors
- Design of the potentiostat and peripheral circuits
- Construction of equivalent circuit
- Fabrication and testing of the potentiostat
- Electrochemical characterization of the dual-channel biosensor with our system
- Dynamic monitoring and stability studies of our system
- Construction of the fully integrated wearable device
- In *vivo* animal experiments
- Ethical approval for in *vivo* experiments

● QUANTIFICATION AND STATISTICAL ANALYSIS

SUPPLEMENTAL INFORMATION

Supplemental information can be found online at https://doi.org/10.1016/j.crmeth.2023.100579.

ACKNOWLEDGMENTS

This work was funded by the National Natural Science Foundation of China, grant no. 82272121 (to H.W.); the National Key R&D Program of China, grant no. 2020YFB2009004 (to H.W.); and the Innovation Team and Talents Cultivation Program of National Administration of Traditional Chinese Medicine, grant no. ZYYCXTD-D-202003 (to H.W.).

AUTHOR CONTRIBUTIONS

M.Y. drafted the manuscript, designed the ultrasensitive wearable biosensor, collected and analyzed the data, and conducted experiments. H.W. designed the study, supervised this work, and drafted and revised the manuscript. J.C. supervised this work and revised the manuscript.

DECLARATION OF INTERESTS

The authors declare no competing interests.

Received: March 20, 2023
Revised: May 17, 2023
Accepted: August 10, 2023
Published: September 6, 2023

REFERENCES

1. International Diabetes Federation (2021). IDF Diabetes Atlas, 10th edn. (Brussels, Belgium: International Diabetes Federation).
2. Hotamisligil, G.S. (2006). Inflammation and metabolic disorders. Nature *444*, 860–867. https://doi.org/10.1038/nature05485.
3. Warrell, D.A., White, N.J., Veall, N., Looareesuwan, S., Chanthavanich, P., Phillips, R.E., Karbwang, J., Pongpaew, P., and Krishna, S. (1988). Cerebral anaerobic glycolysis and reduced cerebral oxygen transport in human cerebral malaria. Lancet *2*, 534–538. https://doi.org/10.1016/s0140-6736(88)92658-x.
4. Clarke, S.F., and Foster, J.R. (2012). A history of blood glucose meters and their role in self-monitoring of diabetes mellitus. Br. J. Biomed. Sci. *69*, 83–93. https://doi.org/10.1080/09674845.2012.12002443.
5. Zhao, H., Qiu, X., Su, E., Huang, L., Zai, Y., Liu, Y., Chen, H., Wang, Z., Chen, Z., Li, S., et al. (2022). Multiple chemiluminescence immunoassay detection of the concentration ratio of glycosylated hemoglobin A1c to total hemoglobin in whole blood samples. Anal. Chim. Acta *1192*, 339379. https://doi.org/10.1016/j.aca.2021.339379.
6. Schmid, T., Baumann, B., Himmelsbach, M., Klampfl, C.W., and Buchberger, W. (2016). Analysis of saccharides in beverages by HPLC with direct UV detection. Anal. Bioanal. Chem. *408*, 1871–1878. https://doi.org/10.1007/s00216-015-9290-1.
7. Chen, J., Xu, Y., Xu, F., Zhang, Q., Li, S., and Lu, X. (2021). Detection of hydrogen peroxide and glucose with a novel fluorescent probe by the enzymatic reaction of amino functionalized MOF nanosheets. Anal. Methods *13*, 4228–4237. https://doi.org/10.1039/d1ay00190f.
8. Ahn, J.W., Ku, Y., and Kim, H.C. (2019). A novel wearable EEG and ECG recording system for stress assessment. Sensors *19*, 1991. https://doi.org/10.3390/s19091991.
9. Wang, Y., Li, B., Tian, T., Liu, Y., Zhang, J., and Qian, K. (2022). Advanced on-site and in vitro signal amplification biosensors for biomolecule analysis. Trends Anal. Chem. *149*, 116565. https://doi.org/10.1016/j.trac.2022.116565.
10. Feng, J., Zhou, C., He, C., Li, Y., and Ye, X. (2017). Development of an improved wearable device for core body temperature monitoring based on the dual heat flux principle. Physiol. Meas. *38*, 652–668. https://doi.org/10.1088/1361-6579/aa5f43.
11. Polat, E.O., Mercier, G., Nikitskiy, I., Puma, E., Galan, T., Gupta, S., Montagut, M., Piqueras, J.J., Bouwens, M., Durduran, T., et al. (2019). Flexible graphene photodetectors for wearable fitness monitoring. Sci. Adv. *5*, eaaw7846. https://doi.org/10.1126/sciadv.aaw7846.
12. Lee, I., Probst, D., Klonoff, D., and Sode, K. (2021). Continuous glucose monitoring systems - Current status and future perspectives of the flagship technologies in biosensor research. Biosens. Bioelectron. *181*, 113054. https://doi.org/10.1016/j.bios.2021.113054.
13. Tehrani, F., Teymourian, H., Wuerstle, B., Kavner, J., Patel, R., Furmidge, A., Aghavali, R., Hosseini-Toudeshki, H., Brown, C., Zhang, F., et al. (2022). An integrated wearable microneedle array for the continuous monitoring of multiple biomarkers in interstitial fluid. Nat. Biomed. Eng. *6*, 1214–1224. https://doi.org/10.1038/s41551-022-00887-1.
14. Wang, Y., Tan, P., Wu, Y., Luo, D., and Li, Z. (2022). Artificial intelligence-enhanced skin-like sensors based on flexible nanogenerators. View *3*, 20220026. https://doi.org/10.1002/VIW.20220026.
15. Yu, Y., Nassar, J., Xu, C., Min, J., Yang, Y., Dai, A., Doshi, R., Huang, A., Song, Y., Gehlhar, R., et al. (2020). Biofuel-powered soft electronic skin with multiplexed and wireless sensing for human-machine interfaces. Sci. Robot. *5*, eaaz7946. https://doi.org/10.1126/scirobotics.aaz7946.
16. Yang, M., Liu, M., Cheng, J., and Wang, H. (2021). A movable type bioelectronics printing technology for modular fabrication of biosensors. Sci. Rep. *11*, 22323. https://doi.org/10.1038/s41598-021-01741-1.
17. Wang, H., Wang, X., and Cheng, J. (2022). Bionic enzyme-assisted ion-selective amperometric biosensor based on 3D porous conductive matrix for point-of-care nitrite testing. ACS Nano *16*, 14849–14859. https://doi.org/10.1021/acsnano.2c05752.
18. Yang, M., Wang, H., Liu, P., and Cheng, J. (2021). A 3D electrochemical biosensor based on Super-Aligned Carbon NanoTube array for point-of-care uric acid monitoring. Biosens. Bioelectron. *179*, 113082. https://doi.org/10.1016/j.bios.2021.113082.
19. Majumdar, S., and Mahanta, D. (2020). Deposition of an ultra-thin polyaniline coating on a TiO_2 surface by vapor phase polymerization for electrochemical glucose sensing and photocatalytic degradation. RSC Adv. *10*, 17387–17395. https://doi.org/10.1039/d0ra01571g.
20. Puttananjegowda, K., Takshi, A., and Thomas, S. (2021). Silicon carbide nanoparticles electrospun nanofibrous enzymatic glucose sensor. Biosens. Bioelectron. *186*, 113285. https://doi.org/10.1016/j.bios.2021.113285.
21. Cai, Y., Liang, B., Chen, S., Zhu, Q., Tu, T., Wu, K., Cao, Q., Fang, L., Liang, X., and Ye, X. (2020). One-step modification of nano-polyaniline/glucose oxidase on double-side printed flexible electrode for continuous glucose

monitoring: characterization, cytotoxicity evaluation and in vivo experiment. Biosens. Bioelectron. *165*, 112408. https://doi.org/10.1016/j.bios.2020.112408.

22. Popov, A., Aukstakojyte, R., Gaidukevic, J., Lisyte, V., Kausaite-Minkstimiene, A., Barkauskas, J., and Ramanaviciene, A. (2021). Reduced graphene oxide and polyaniline nanofibers nanocomposite for the development of an amperometric glucose biosensor. Sensors *21*, 948. https://doi.org/10.3390/s21030948.
23. Liu, X., Zhang, W., Lin, Z., Meng, Z., Shi, C., Xu, Z., Yang, L., and Liu, X.Y. (2021). Coupling of silk fibroin nanofibrils Enzymatic membrane with ultrathin PtNPs/Graphene film to acquire long and stable on-skin sweat glucose and lactate sensing. Small Methods *5*, e2000926. https://doi.org/10.1002/smtd.202000926.
24. Madden, J., Vaughan, E., Thompson, M., O' Riordan, A., Galvin, P., Iacopino, D., and Rodrigues Teixeira, S. (2022). Electrochemical sensor for enzymatic lactate detection based on laser-scribed graphitic carbon modified with platinum, chitosan and lactate oxidase. Talanta *246*, 123492. https://doi.org/10.1016/j.talanta.2022.123492.
25. Han, J.H., Hyun Park, S., Kim, S., and Jungho Pak, J. (2022). A performance improvement of enzyme-based electrochemical lactate sensor fabricated by electroplating novel PdCu mediator on a laser induced graphene electrode. Bioelectrochemistry *148*, 108259. https://doi.org/10.1016/j.bioelechem.2022.108259.
26. Tsou, K.L., Chen, K.Y., Chou, Y.D., Cheng, Y.T., Tsai, H.E., and Lee, C.K. (2022). Inkjet-printed flexible non-enzymatic lactate sensor with high sensitivity and low interference using a stacked NiOx/NiOx-Nafion nanocomposite electrode with clinical blood test verification. Talanta *249*, 123598. https://doi.org/10.1016/j.talanta.2022.123598.
27. Neampet, S., Ruecha, N., Qin, J., Wonsawat, W., Chailapakul, O., and Rodthongkum, N. (2019). A nanocomposite prepared from platinum particles, polyaniline and a Ti_3C_2 MXene for amperometric sensing of hydrogen peroxide and lactate. Mikrochim. Acta *186*, 752. https://doi.org/10.1007/s00604-019-3845-3.
28. Heikenfeld, J., Jajack, A., Feldman, B., Granger, S.W., Gaitonde, S., Begtrup, G., and Katchman, B.A. (2019). Accessing analytes in biofluids for peripheral biochemical monitoring. Nat. Biotechnol. *37*, 407–419. https://doi.org/10.1038/s41587-019-0040-3.
29. Yoon, J., Lee, S.N., Shin, M.K., Kim, H.W., Choi, H.K., Lee, T., and Choi, J.W. (2019). Flexible electrochemical glucose biosensor based on GOx/gold/MoS2/gold nanofilm on the polymer electrode. Biosens. Bioelectron. *140*, 111343. https://doi.org/10.1016/j.bios.2019.111343.
30. Skoog, D.A., and West, D.M. (1982). Fundamentals of Analytical Chemistry, 4th ed. (Saunders College Publishing).
31. Laschuk, N.O., Easton, E.B., and Zenkina, O.V. (2021). Reducing the resistance for the use of electrochemical impedance spectroscopy analysis in materials chemistry. RSC Adv. *11*, 27925–27936. https://doi.org/10.1039/d1ra03785d.
32. Panayotov, I.V., Orti, V., Cuisinier, F., and Yachouh, J. (2016). Polyetheretherketone (PEEK) for medical applications. J. Mater. Sci. Mater. Med. *27*, 118. https://doi.org/10.1007/s10856-016-5731-4.
33. Verma, S., Sharma, N., Kango, S., and Sharma, S. (2021). Developments of PEEK (Polyetheretherketone) as a biomedical material: a focused review. Eur. Polym. J. *147*, 110295. https://doi.org/10.1016/j.eurpolymj.2021.110295.
34. Miller, P.R., Taylor, R.M., Tran, B.Q., Boyd, G., Glaros, T., Chavez, V.H., Krishnakumar, R., Sinha, A., Poorey, K., Williams, K.P., et al. (2018). Extraction and biomolecular analysis of dermal interstitial fluid collected with hollow microneedles. Commun. Biol. *1*, 173. https://doi.org/10.1038/s42003-018-0170-z.

STAR★METHODS

KEY RESOURCES TABLE

REAGENT or RESOURCE	SOURCE	IDENTIFIER
Chemicals, peptides, and recombinant proteins		
Nafion	Sigma (Steinheim, Germany)	Cas: 31175-20-9
Glucose	Sigma (Steinheim, Germany)	Cas: 50-99-7
Lactate acid	Sigma (Steinheim, Germany)	Cas: 50-21-5
Glutaraldehyde solution (50% in H_2O)	Sigma (Steinheim, Germany)	Cas: 111-30-8
Potassium ferricyanide ($K_3[Fe(CN)_6]$)	Aladdin (Shanghai, China)	Cas: 13746-66-2
Potassium hexacyanoferrate(II) ($K_4Fe(CN)_6$)	Aladdin (Shanghai, China)	Cas: 14459-95-1
Potassium chloride (KCl)	Aladdin (Shanghai, China)	Cas: 7447-40-7
Glucose oxidase (10 units/mg)	Yuanye Bio-Technology Corporation (Shanghai, China)	Cas: 9001-37-0
Lactate oxidase (36 units/mg)	Yuanye Bio-Technology Corporation (Shanghai, China)	Cas: 9028-72-2
Software and algorithms		
MATLAB 2014	MathWorks (Natick, MA)	https://www.mathswork.com
Origin 8.0	OriginLab Corporation (Northampton, MA)	https://www.originbab.com
Multisim 14.0	National Instruments Corporation (Austin, TX)	https://www.ni.com
Altium Designer 19.0	Altium Corporation (Hobart, Australia)	https://www.altium.com.cn/altium-designer/
Apparatus		
Electrochemical workstation	Chenhua (Shanghai, China)	CHI660E
Other		
Polydimethylsiloxane (PDMS)	Dow Corning Corporation	Sylgard 184
Ag conductive paste	Ausbond Corporation (Shenzhen, China)	3813
Carbon paste	Ausbond Corporation (Shenzhen, China)	A528
Nickel foam	Guangshengjia New Materials Company (Kunshan, China)	GSJ76851
Polyethylene terephthalate (PET)	Suzhou Gule Packaging Materials Company (Suzhou, China)	CAS: 25038-59-9

RESOURCE AVAILABILITY

Lead contact

Requests for resources and additional information should be directed to and will be fulfilled by the lead contact, Dr. Han Wang (hanwang@tsinghua.edu.cn).

Materials availability

This study did not generate new unique reagents.

Data and code availability

- All data reported in this paper will be shared by the lead contact upon request (hanwang@tsinghua.edu.cn).
- This paper does not report original code.
- Any additional information required to reanalyze the data reported in this paper is available from the lead contact upon request (hanwang@tsinghua.edu.cn).

EXPERIMENTAL MODEL AND STUDY PARTICIPANT DETAILS

A ten-month-old female adult mouse on a BALB/c background was used in this study. The laboratory mouse was housed, when possible, on a 12-h light/dark cycle in ventilated racks inside a humidity-controlled room with RH 40–55% and a temperature range of 21°C–23°C. The mouse had *ad libitum* access to food and water. The sex and gender of the mice rarely influenced the results of the

study, which aimed to assess the feasibility of the proposed wearable device. The *in vivo* animal experiments were approved and conducted under the guidance and supervision of the Laboratory Animal Center of Tsinghua University. The reporting of this work complies with ARRIVE guidelines.

METHOD DETAILS

Electrochemical detection mechanism of the 3D-structured nickel foam electrode

The developed enzyme-modified 3D-structured Nickel foam electrochemical biosensor is based on the three-electrode scheme. First, glucose and lactate in the interstitial fluids are oxidized by corresponding oxidase and generate H_2O_2. Then H_2O_2 is rapidly oxidized with the help of catalyst nickel under appropriate potential. The electrons lost by H_2O_2 are transferred to 3D-structured Nickel foam and the corresponding current can be detected by our fabricated potentiostat. The following chemical Equations 1, 2 and 3 show the detailed detection mechanism of glucose and lactate on 3D-structured Nickel foam electrode.

$$\text{Glucose} + O_2 \xrightarrow{GO_x} \text{Gluconate} + H_2O_2 \quad \text{(Equation 1)}$$

$$\text{Lactate} + O_2 \xrightarrow{LO_x} \text{Pyruvate} + H_2O_2 \quad \text{(Equation 2)}$$

$$2H_2O_2 \rightarrow O_2 + 4H^+ + 4e^- \quad \text{(Equation 3)}$$

GO_x refers to glucose oxidase and LO_x refers to lactate oxidase. Then, the produced H_2O_2 decomposes on the surface of the 3D-structured Nickel foam electrodes and the corresponding current is detected to calculate the concentration of glucose and lactate, respectively.

Fabrication of the dual-channel 3D-structured biosensors through a movable type bioelectronics printing technology

A dual-channel biosensor for glucose and lactate monitoring was fabricated by the movable type bioelectronics printing technology, which includes the following steps. Firstly, we transfer printed the counter electrode and working electrode with conductive carbon paste and transfer printed linking wires and reference electrode with Ag/AgCl paste. After drying the conductive electrodes in the ventilating oven at 40°C for 30 min, we transfer printed the protective Nafion layer for enzymes and the insulator layer step by step. After that, 3D-structured Nickel foam were immobilized on the working electrode with conductive carbon paste under 115°C for 15 min and then lactate oxidase and glucose oxidase were prepared to modify the two working electrodes.

Enzyme modification of dual-channel 3D-structured biosensors

For immobilization of lactate oxidase, chitosan/CNTs solution was prepared by adding 5 mg amino functionalized carbon nanotubes into a 2 mL chitosan solution (0.2% wt) with ultrasonic mixing for 10 min to achieve complete dispersion. Then 1 mg lactate oxidase was added to Chitosan/CNTs solution (50 μL) to obtain Lactate oxidase/Chitosan CNTs solution. A drop of Lactate oxidase/Chitosan CNTs solution (3 μL) was introduced onto one of the working electrodes, dried at room temperature, and then 3 μL glutaraldehyde solution (5%) was added onto the working electrode. The above mixture was incubated at room temperature to crosslink for 1 h, and the lactate oxidase-modified electrode was thus prepared. The other working electrode was modified with the same procedures, only replacing lactate oxidase with glucose oxidase. Finally, the dual-channel biosensor was gently rinsed 3 times with PBS by pipetting and stored in refrigerator at 4°C until use.

Design of the potentiostat and peripheral circuits

The potentiostat module connected with a three-electrode biosensor is shown in Figure S2. The main function of the potentiostat module is to maintain a constant voltage between the working electrode and the reference electrode in the electrochemical cell, and measure the reaction current on the working electrode. To realize this function, an equivalent circuit model of the three-electrode biosensor was constructed.

The circuit of potentiostat was designed based on the equivalent circuit to maintain the potential ($U_{RE\text{-}WE}$) between the working electrode and the reference electrode. During the electrochemical reaction, current was generated between the working electrode and the counter electrode, to offset the difference between the preset potential and the actual potential of the working electrode. The operational amplifier connected with the reference electrode acted as a voltage follower, since the input resistance of operational amplifier was approximately infinite. The infinite input resistance kept the voltage of the reference electrode constant. Through maintaining constant potential of the operational amplifiers, the potentiostat can generate constant voltage between the working electrode and the reference electrode of the three-electrode sensor in the electrochemical detection system. Meanwhile, the current passing through the working electrode can be measured for both qualitative and quantitative analysis of the electrochemical reaction for target analytes.

Construction of equivalent circuit

The equivalent circuit including its structure and parameters could be simulated via electrical impedance spectroscopy (EIS). EIS is a highly sensitive technique capable of characterizing the electrical response of electrochemical systems in a nondestructive manner.

The electrolytic cell of a typical electrochemical system consists of electrodes and the electrolyte solution. In the electrolytic cell, the electric double layer can be equivalently regarded as a capacitor. And the resistance caused by the electrode, solution and electrode reaction can be regarded as equivalent resistors. Therefore, the equivalent circuit of the entire electrolytic cell can be represented as in Figure S2B. C_2 and C_3 represent the electric double layer capacitance of the working electrode and the counter electrode, respectively. Z_1 and Z_2 represent the alternating current (AC) impedance (also called Faraday impedance) of the working electrode and the counter electrode, respectively. R represents the equivalent resistance of the electrolytic solution, and C_1 represents the capacitance of the electrolyte solution between the working electrode and the counter electrode.

Regardless of the shape of the electrolytic cell, the distance between the working electrode and the counter electrode is typically hundreds of times larger than the thickness of the electric double layer capacitor. Therefore, the complex impedance in circuit branch with C_1 is much larger than that in the other circuit branch with C_2, so capacitance C_1 can be omitted. Typically, no electrochemical reaction occurs on the counter electrode and the area of the counter electrode is much larger than that of the working electrode, thus Z_2 and C_3 could be very large. Therefore, the interface impedance of the counter electrode can be ignored. Moreover, the Faraday impedance of the electrolytic cell includes two parts, the electrode polarization resistance R_P and the concentration polarization resistance Warburg impedance Z_w. Thus, the equivalent circuit of the electrochemical biosensor can be simplified as in Figure S2B.

Mathematically, the total impedance of the equivalent circuit can be written in complex form by Equation 1 [30]:

$$Z = R + \frac{1}{j_w C_2 + \frac{1}{R_p + \sigma\omega^{-\frac{1}{2}}(1 - j)}}$$

According to the EIS results and Nyquist curve fitting, the parameters of the corresponding components in the equivalent circuit can be calculated.[31]

Fabrication and testing of the potentiostat

EIS testing of a bare three-electrode biosensor as control, and another three-electrode biosensor with Nickel foam by a commercial electrochemical workstation (CHI660E, Chenhua, Shanghai, China) was conducted to help analyze the equivalent circuit of biosensors. EIS tests were conducted in 1 mM $Fe(CN)_6^{3-/4-}$ (1:1) solution containing 0.1 M KCl and the Nyquist spectrograms were recorded in order. According to the EIS results and Nyquist curve fitting, the parameters of the corresponding components in the equivalent circuit were calculated by ZView 3.1 (Scribner Associates, Inc., North Carolina, USA). Then a simulation software Multisim (Multisim 14.0, National Instruments Corporation, Austin, TX) was applied to simulate and test the designed potentiostat module with an equivalent circuit model of the three-electrode biosensor. After simulation, the detection system was designed with Altium Designer (Altium Designer 19.0, Altium Corporation, Hobart, Australia) and fabricated by a PCB manufacturer (Shenzhen Jialichuang Corporation, Shenzhen, China). After soldering components on the fabricated PCB, experiment tests of the potentiostat connected with a three-electrode biosensor in PBS were conducted to verify the feasibility of the potentiostat.

Electrochemical characterization of the dual-channel biosensor with our system

To further evaluate the performance of the dual-channel biosensor for lactate and glucose detection, amperometric i-t curves were recorded after injecting 100 μL mixed solutions with lactate and glucose into the working electrode at room temperature (25°C). After each measurement, the working electrode was cleaned three times with DI water. The potential of amperometric i-t tests was set at 0.30 V and the testing time was set to 100 s. All data was processed using MATLAB 2014 (MathWorks, Natick, MA) and Origin 8.0 (OriginLab Corporation, Northampton, MA).

Dynamic monitoring and stability studies of our system

To evaluate the dynamic monitoring performance of the dual-channel biosensor, amperometric i-t curve for measuring lactate and glucose at different concentrations in PBS solution (pH = 7.4) was tested. Series of lactate and glucose samples with different concentrations were prepared and introduced into the working electrode respectively. The applied potential was 0.12 V. The flow rate was 50 μL/min.

Construction of the fully integrated wearable device

The fully integrated wearable device consisted of six modules including the adhesive layer, base box, dual-channel biosensor, microneedle, circuit board and cover, which can detect and transmit real-time data to electronic terminals. All the modules were compatibly integrated into a wearable device. The size of the device was 3 × 5 × 0.5 cm^3 with a total weight of 40 g. Specifically, the base box and cover plate of the device were constructed through 3D printing of polytetrafluoroethylene (PTFE), and the medical double-sided adhesive was used as the adhesive layer to fix the device on the surface of the skin. Besides, the microneedle used in this work was

customized by biocompatible polyether-ether-ketone (PEEK)[32,33] with 70 μm inner diameter. The interstitial fluid was extracted to the detection chamber, in virtue of the negative pressure generated by the PEEK microneedle after penetrating through the skin.[34] Additionally, the dual-channel biosensor was first fabricated through the steps mentioned above, connected with the circuit board, and then integrated into the wearable device.

In *vivo* animal experiments

The proposed wearable device was attached to a health mouse and a PEEK tube was inserted into the blood vessel in the tail of the animals. The monitoring results of lactate and glucose were recorded for a total of 2 h. For comparison, blood samples were collected every 10 min and detected by FDA-approved electrochemical glucose analyzer (Accu-Chek Advantage, Roche Diagnostics Corporation, Basel, Switzerland) and lactate analyzer (Lactate Scout 4, EKF Diagnostics Corporation, Barleben, Germany), respectively.

Ethical approval for in *vivo* experiments

The *in vivo* animal experiments were approved and conducted under the guidance and supervision of Laboratory Animal Center of Tsinghua University.

QUANTIFICATION AND STATISTICAL ANALYSIS

Statistical analysis of the data was conducted in Microsoft Office Excel, MATLAB 2014 and Origin 8.0. Figures were prepared with Adobe Illustrator (version 27.4, Adobe) and Microsoft Office Power Point. All p values <0.05 were considered statistically significant. Error bars in all plots represent mean ± standard deviation with the number of replicates indicated in the figure legends. Statistical analysis of Figures 5A, 5C and 6D was conducted by paired t-test.